Computational fluid dynamics in the numerical simulation analysis of end-to-side anastomosis for coarctation of the aorta

Fang Yang[1#], Bo Zhai[1#], Li-Gong Hou[2], Qian Zhang[3], Jie Wang[3]

[1]Department of Cardiac Surgery, [2]Department of Teaching, [3]Department of Surgery, Henan Children's Hospital, Zhengzhou Children's Hospital, Zhengzhou 450018, China

Contributions: (I) Conception and design: F Yang, B Zhai, J Wang; (II) Administrative support: J Wang; (III) Provision of study materials or patients: F Yang, B Zhai, J Wang; (IV) Collection and assembly of data: LG Hou; (V) Data analysis and interpretation: Q Zhang; (VI) Manuscript writing: All authors; (VII) Final approval of manuscript: All authors.

[#]These authors contributed equally to this work.

Correspondence to: Jie Wang. Department of surgery, Henan Children's Hospital, Zhengzhou Children's Hospital, No. 33 of Waihuan Road, Zhengdong New District, Zhengzhou 450018, China. Email: jiewang_dr@163.com.

Background: Based on CT image data, a computational fluid dynamics (CFD) model of the aortic arch was established. We aimed to investigate the hemodynamic features associated with end-to-side anastomosis (ESA) surgery for coarctation of the aorta (CoA) by CFD model.

Methods: The data of enhanced CT two-dimensional medical images obtained through clinical practice were processed using medical image post-processing software. The three-dimensional model of the aortic arch was obtained through the geometric model and boundary condition. This was subsequently transformed into a CAD model, which can be used for simulation calculation.

Results: The CFD model accurately reflected the shape of the aortic arch, and produced the hemodynamic results before and after ESA for CoA.

Conclusions: The CFD model provides a virtual execution platform for the scientific research of aortic arch disease and will be helpful to evaluate the operation plan, even to determine the best surgical procedure. Hemodynamic analysis may be helpful to evaluate the therapeutic effects of other aortic diseases.

Keywords: Aortic coarctation; end-to-side aortic anastomosis (EASS); computational fluid dynamics (CFD)

Introduction

With the development of computing technology, numerical calculation has been widely used to simulate complex flows of various real shapes. The core task of computational fluid dynamics (CFD) is to solve the problem by numerical discretization and solution approaches in order to obtain the numerical solution of the discrete time/space points in the flow field. Due to the strengthening of cooperation among different disciplines, CFD has been widely used in the fields of hemodynamic assessment, post-operative regional blood flow evaluation and surgical simulation. Based on the development of medical imaging technology and its corresponding medical processing software, the numerical simulation of blood flow by CFD method has been widely popularized. Hence, the investigators attempted to determine the right combination point and set reasonable calculation conditions, in order to numerically simulate different surgical procedures for coarctation of the aorta (CoA), and further analyze the indexes. This would be helpful for the surgeon to have certain sensory verification before and after the operation, and select the best operation plan. The general structure of the CFD software includes three parts: pre-processing, solver, and post-processing (1). Pre-processing includes the geometric model and mesh partition (2). Solver mainly consists of the control equations
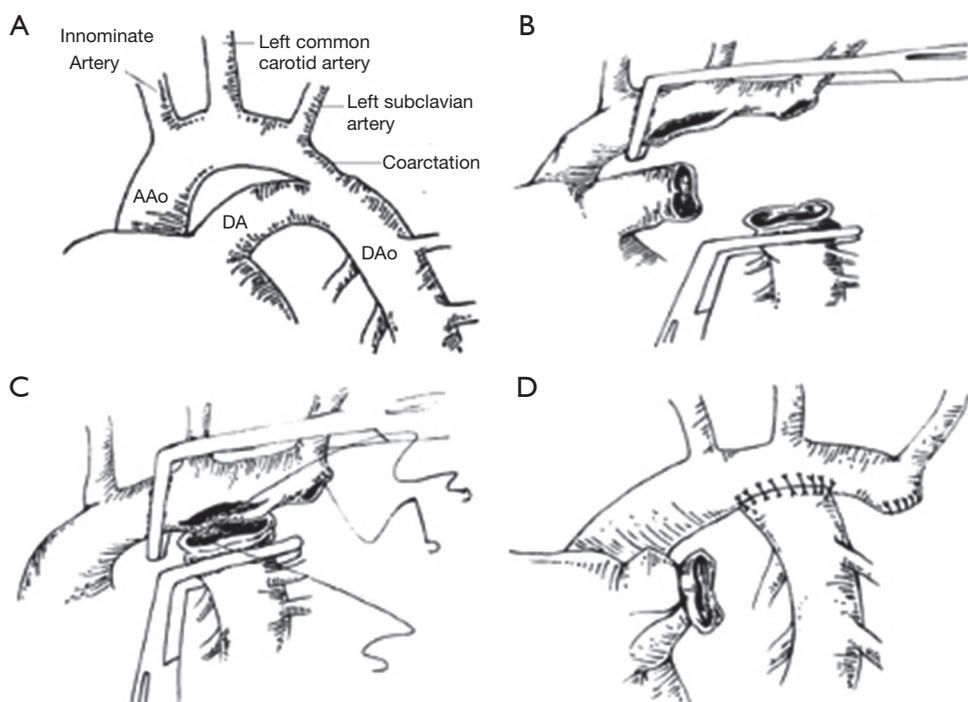
Figure 1 Aortic arch constriction end-to-side aortic anastomosis. Basic anatomy (A); the first stage of the operation (B); the second stage of the operation (C); corrected results (D). AAo, ascending aorta; DAo, descending aorta; DA, ductus arteriosus.

for determining the CFD method, the proper discrete method, and the proper numerical calculation method and the related parameters to input (3). Post-processing refers to the CFD calculation, in which the results displayed are carried out separately, and there is no interaction between these two.

CoA is a kind of the common congenital heart diseases. Recently, surgery, percutaneous transluminal angioplasty (PTA) are recommended as a primary treatment for aortic coarctation. Such as surgical repair of CoA through left thoracotomy, balloon dilation, endovascular stent placement. In clinical practice, once aortic constriction is diagnosed, it can be treated by surgery with or without symptoms. Balloon dilation and endovascular stent placement are simple and have low mortality. From the clinical point of view, balloon dilation can be used as an alternative to the surgical treatment of aortic constriction. The incidence of CoA in newborns is 0.2–0.6/1,000, and accounts for 5–8% of all patients with congenital heart disease (1,2). With the development of surgical procedures, proper surgical correction in childhood has been considered the first choice for the treatment of CoA. However, there are controversies on the optimal management of CoA about

the choice of the best age for the operation; the effects of different anastomosis procedures on the aortic arch flow, and how to deal with related aortic arch hypoplasia (3). End-to-side anastomosis (ESA) was one of the most ideal procedures of ESA for CoA and tubular hypoplasia of the aortic arch which was first proposed by Rajasinghe *et al.* in 1996. The main procedure of ESA is to excise the coarctation segment and expand the anastomosis between the descending aorta and arch of the aorta. In this process (4,5), all abnormal tissue of the aorta, such as ductal and tubular tissues with incomplete development, are completely removed (6-10) (*Figure 1*).

Based on computed tomography (CT) image data, a CFD model of the aortic arch was established. Therefore, we conducted this study to investigate the hemodynamic features associated with ESA surgery for CoA by CFD model in order to obtain the rules of individualized treatment and assess the ESA program.

Methods

Our hospital is the largest children's hospital in Henan province. The clinical data were obtained from the medical

6580

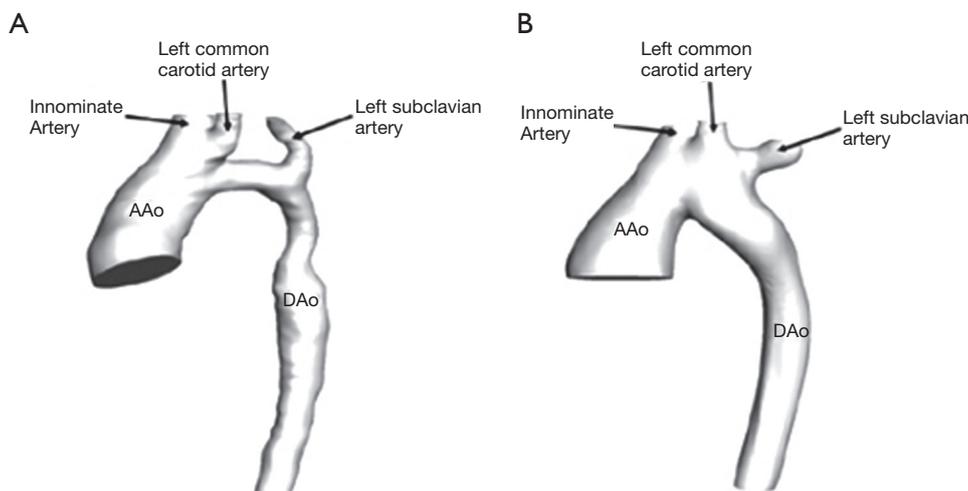Yang et al. CFD in analyzing ESA for CoA

A

B

Figure 2 Vascular morphology: pre-operation (A); post-operation (B). AAo, ascending aorta; DAo, descending aorta.

database which imported the data of thousands of surgical patients each year. With the consent of the patients and their parents, structural regional images were extracted from the preoperative CT and magnetic resonance (MRI) data. We collated and analyzed clinical data from the medical database and started conducted this retrospective study in May 2015. The research protocol was conducted in accordance with the guidelines of the World Medical Association's Declaration of Helsinki, and performed following the approval of the Medical Ethics Committee of Henan Children's Hospital (No. 20140307).

Image data

In our study, we randomly selected a patient with preoperative and postoperative diagnosis of narrow aortic arch and extensive anastomosis, data was obtained from children who was 40 days old. The CT images were stored in DICOM format, the slice gap was 2.5 mm, the two-dimensional resolution of each layer was 512×512, and the pixel size was 0.5 mm. Then, the CT images were imported into the medical image post-processing software Mimics 16.0 to reconstruct the 3D geometric model. On the images, tissues, except for the aortic arch, were removed using the automatic threshold segmentation method and through manual separation. Hence, the three-dimensional models of the structure, including the three branches of the ascending aorta, aortic arch and descending aorta, as well as the upper part of aortic arch (including the brachiocephalic trunk, left common carotid artery and left subclavian

artery), were obtained. *Figure 2* simulates the vascular structure in the pre- and post-operative state of the child.

Numerical analysis

For the properties of the materials, data were usually provided by related biomechanical studies. The heterogeneity and nonlinearity of the biological structures were usually described in a homogeneous and linear manner in the study. Although such simplification may affect the pressure distribution in structural studies, it did not produce a significant difference in the description of characteristics of the whole model. It was assumed that the arterial blood flow was a laminar, incompressible Newtonian fluid, the blood vessels were rigid and non-permeable, without a sliding on wall, and the elasticity and thickness of the arterial wall were neglected (2). Newtonian fluid density $\rho=1,060 \text{ kg/m}^3$, and the viscosity coefficient was $\mu=4.0\times10^{-3}$ Pa.S. The Navier-Stokes equation for the conservation of momentum of incompressible fluid was solved by CFD calculation.

$$\frac{\partial}{\partial t}(\rho\mu_i) + \frac{\partial}{\partial \chi_j}(\rho\mu_i\mu_j) = \frac{\partial\rho}{\partial t} + \frac{\partial}{\partial \chi_j}(\rho\mu_i) = 0 \qquad [1]$$

Eq. [1]: i, j =1,2,3; X represent the axis of the coordinate; u_i, u_j represents the velocity vector; p represents pressure; μ represents the coefficient of viscosity; ρ represents density, and t represents time.

Previous studies have revealed that the blood flow in the aortic arch was a turbulent flow. Therefore, the most widely

used turbulence model, k-ε, was used to solve the complex pulsating flow. The κ-ε formulae are listed as follows:

Eddy viscosity Eq. [2]:

$$\mu = \rho C_\mu \frac{k^2}{\varepsilon} \qquad [2]$$

Turbulence momentum Eq. [3]:

$$\rho \frac{\partial k}{\partial t} + \rho \mu_j \frac{\partial k}{\partial x_j} = \tau_{ij} \frac{\partial u_i}{\partial x_j} - \rho \varepsilon + \frac{\partial}{\partial x_j} \left\{ \left(\mu + \frac{\mu_t}{\sigma_k} \right) \frac{\partial k}{\partial x_j} \right\} \qquad [3]$$

Energy consumption rate formula for turbulence Eq. [4]:

$$\rho \frac{\partial \varepsilon}{\partial t} + \rho \mu_j \frac{\partial k}{\partial x_j} = C_{\varepsilon 1} \frac{\varepsilon}{k} \tau_{ij} \frac{\partial u_i}{\partial x_j} - C_{\varepsilon 2} \rho \frac{\varepsilon^2}{k} + \frac{\partial}{\partial x_j} \left\{ \left(\mu + \frac{\mu_t}{\sigma_\varepsilon} \right) \frac{\partial \varepsilon}{\partial x_j} \right\}$$
$$[4]$$

Termination coefficients: $C_{\varepsilon 1} = 1.44$, $C_{\varepsilon 2} = 1.92$, $C_U = 0.09$, $\sigma_k = 1.0$, $\sigma_\varepsilon = 1.3$

Grid partition

The blood flow described by the numerical equation was meshed using the commercial software ANSYS 14.0. The tetrahedral mesh was divided into 1,049,540 units and 521,283 nodes before the operation, while the tetrahedral mesh was divided into 1,058,498 units and 532,755 nodes.

Boundary condition

Boundary conditions were used to define the parameters of the model, and the relationship between the model and its surrounding tissues. In the experiment, the boundary conditions could be set based on relatively real data, because when the boundary condition was inaccurate, it would lead to false results (11). As much as possible, the clinical data of blood flow and pressure were obtained and used. Mass flow refers to the fluid mass passing through the effective section of closed pipe or open groove per unit of time. In our study, the mass flow of the ascending aorta before and after the operation was obtained by analyzing the CT, and the numerical data were extracted and stored in ASCII format. In order to fully form the flow boundary layer at the entrance and restore the outlet pressure, the investigators expanded the up-flow area at the entrance to 20 times the size of the ascending aorta. Furthermore, in the normal flow direction, each branch unit was expanded by 60 times. The flow of the pulsating mass represented the inflow. The

zero pressure gradient and pressure wave were applied at the exit (12).

Calculation

The CFD calculation methods based on the numerical simulation mainly included the finite difference method, finite volume method, finite element method and finite analytic method. Among these, the finite volume method had the best adaptability for the irregular area, which is one of the most commonly used numerical methods for the finite element flow field. The investigators assumed that the blood vessels were set as rigid, impermeable, Newtonian fluid, without sliding on the wall, and the twi-difference algorithm was used for the analysis (2). The control equation was used for pulsating simulation.

Results

In our study, we collated and analyzed clinical data from the medical database and started conducted this retrospective study in May 2015. We randomly selected a patient with preoperative and postoperative diagnosis of narrow aortic arch and extensive anastomosis, data were obtained from children who were 40 days old.

Based on CT image data, a CFD model of the aortic arch was established. The results were the description of the flow field and the distribution of the physical quantities. The physical quantities involved in CFD included pressure, velocity, shunt ratio (which is defined as the ratio between the inflow volume through the shunt pipe and the inflow volume through the inlet pipe) and energy loss (which is defined as fluid energy as heat loss and dissipation). CFD visualization supports the three-dimensional display of these physical quantities.

As shown in *Figure 3A*, hypoplasia of the aortic arch was found before the operation, where blood flow had difficulties in passing through the narrow blood vessels. This led to higher pressure in the ascending aorta by approximately 20 mmHg, while lower pressure was induced in the descending aorta. The *Figure 3B* revealed that after the operation, more uniform pressure was assigned to the points in the aorta. In addition, it was observed that the difference in pressure between the entrance and exit after the operation was lower than that in the preoperative model. These results reveal that ESA effectively reduced the dense area of the pressure, and completely matched the clinical measurements.
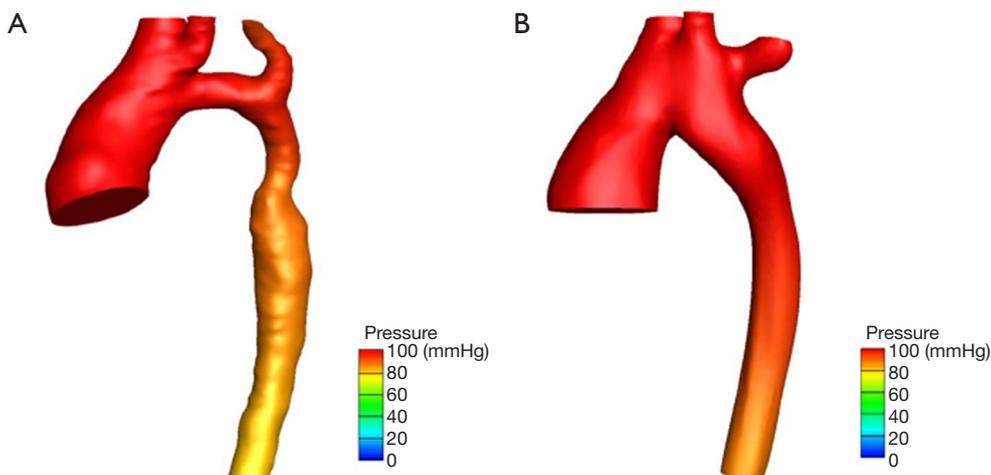
6582

Yang et al. CFD in analyzing ESA for CoA

Figure 3 Pressure distribution: pre-operation (A); post-operation (B).
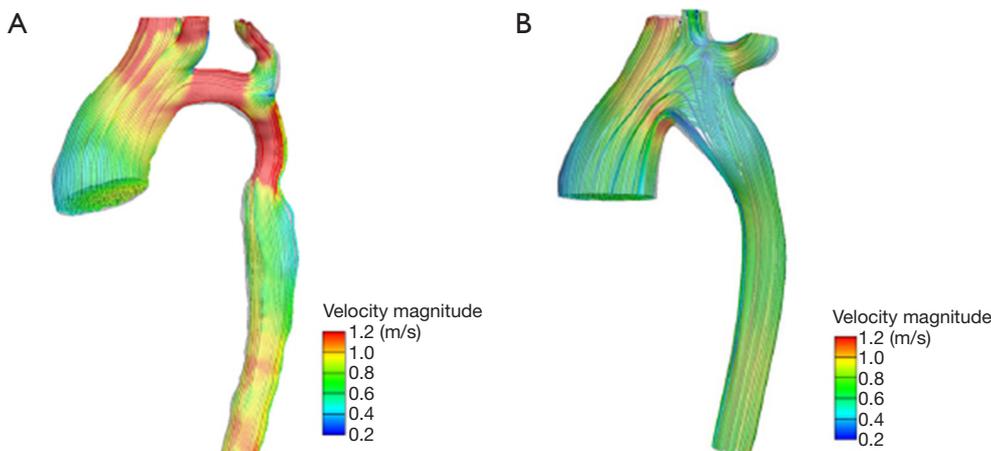

Figure 4 Streamline distribution: pre-operation (A); post-operation (B).

Table 1 The comparison of energy loss in a cardiac cycle between pre-operation and post-operation

Model	Pre-operation	Post-operation
Energy loss (mW)	3.76	2.85

Figure 4A presented the trend of the streamline of the model before the operation. *Figure 4B* presented the trend of the streamline of the model after the operation. The highest dense area was located in the arch with hypoplasia. This also appeared at the systolic peak value before the operation in *Figure 4A*. It is noteworthy that sudden changes in velocity may produce high energy losses in these areas, while blood flow was relatively smooth after the

operation. The *Table 1* presented that the mean energy loss decreased from 3.76 to 2.85 mW in a cardiac cycle and the ESA procedure effectively decreased the workload of the heart.

Figure 5 presented the shunt ratio before and after the operation through the determination of the exit flow/entrance flow. Before the ESA, the mass flow in the descending aorta accounted for 45.9% of the total cardiac output. After the operation, the proportion increased to 52.3% of the total cardiac output. Due the influence of ESA (13), the mass flow in both the innominate artery (IA) and left common coronary artery (LCCA) decreased to a certain extent. This result suggests that the symptoms caused by lack of blood supply in children were relieved.
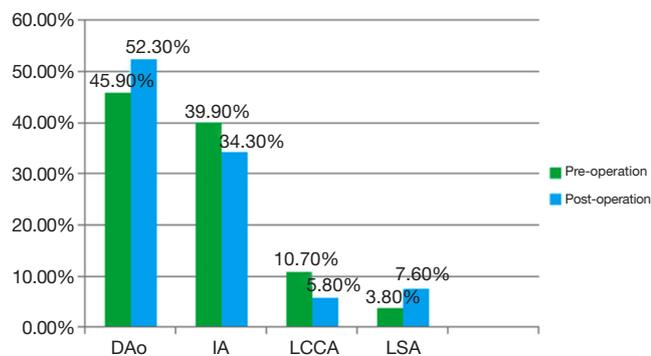
Figure 5 Shunt ratio. DAo, descending aorta; IA, innominate artery; LCCA, left common coronary artery; LSA, left subclavian artery.

Discussion

The outcomes of our study presented that a CFD model of the aortic arch was established based on CT image data. ESA effectively reduced the dense area of the pressure, and completely matched the clinical measurements. These sudden changes in velocity may produce high energy losses in these areas, while blood flow was relatively smooth after the operation. Besides, ESA effectively increased the mass flow in the descending aorta and the mass flow in both the IA and LCCA decreased to a certain extent.

The ESA procedure for CoA can effectively correct the hypoplasia of the aortic arch by reconstructing the aortic arch and removing other abnormal tissues. What needs illustration is that blood vessels were set as rigid flow as laminar inflow rates—neglected elasticity of vessels and flow fluctuates due to heartbeat and cyclic change of intrathoracic pressure caused by respiratory movement. Steady inflow boundary conditions may reduce the flow complexity of flow features and decrease power losses calculated. In addition, collateral flow might influence results.

A former study conducted by Chen *et al.* (14) investigated a hemodynamic model of aortic and ductal arches using CFD and 3D/4D spatiotemporal image correlation (STIC) fetal echocardiography. The results showed that the aortic and ductal arch geometry and flow lead to the alterations in flow profile, velocity, pressure, and wall shear stress (WSS) in the aortic isthmus in normal and CoA models, which are conductive of ductal issue migration into these areas. Another former study conducted by Goubergrits *et al.* (15)

found that peak systolic pressure drops can be reliably calculated using MRI-based CFD in a clinical setting and CFD might be an attractive noninvasive alternative to diagnostic catheterization. However, the hemodynamic features associated with ESA surgery for CoA by CFD model remains unknown. Therefore, we conducted this study and our study presented that the ESA surgery were evaluated through the hemodynamic parameters, such as pressure distribution, WSS distribution, energy loss, and shunt ratio before and after the operation. These indicators demonstrated that ESA is an effective method for the treatment of CoA.

Furthermore, the results of the present study revealed that pressure and energy loss decreased after the operation, providing more blood supply to systemic circulation in order to meet the needs of the body. This also leaded to a reduction in the workload of the heart (16). The data before and after ESA were obtained through CFD simulation for comparative analysis. The visualization results of the pressure distribution and streamline distribution of the vessel wall at blood flow in the two different states, and hemodynamic parameters were obtained, such as energy loss in a cardiac cycle. Furthermore, this technique can be used for the simulation of end-to-end anastomosis and the hemodynamic analysis of ESA with different materials (17). Younoszai *et al.* (8) performed an 88-patient intermediate term follow-up of ESAA for CoA. In their study, they evaluated the procedure of ESA from the viewpoint of clinical treatment and pointed out that the ESAA was an efficacious surgical method for the repair of aortic coarctation. The present study has great guiding significance in establishing individualized operation simulations and the assessment of the best surgical program.

Limitations

Firstly, the sample size of our study is limited and need further research with large sample size. Secondly, the comparison between MRI-based CFD and CT-based CFD remains unknown and need further research. Thirdly, different surgical strategies may have different outcomes. In our study, no information about the difference between the end-to-end surgery and end-to-side surgery was reported.

Conclusions

The CFD model provides a virtual execution platform for

6584

Yang et al. CFD in analyzing ESA for CoA

the scientific research of aortic arch disease and will be helpful to evaluate the operation plan, even to determine the best surgical procedure. Hemodynamic analysis may be helpful to evaluate the therapeutic effects of other aortic diseases.

Acknowledgements

Footnote

Conflicts of Interest: The authors have no conflicts of interest to declare.

Ethical Statement: The research protocol was conducted in accordance with the guidelines of the World Medical Association's Declaration of Helsinki, and performed following the approval of the Medical Ethics Committee of Henan Children's Hospital (No. 20140307)

References

1. Ferencz C, Rubin JD, McCarter RJ, et al. Congenital heart disease: prevalence at livebirth. The Baltimore-Washington Infant Study. Am J Epidemiol 1985;121:31-6.

2. Roger VL, Go AS, Lloyd-Jones DM, et al. Heart disease and stroke statistics--2011 update: a report from the American Heart Association. Circulation 2011;123:e18-209.

3. Jonas RA. Comprehensive Surgical Management of Congenital Heart Disease. J R Soc Med 2004;97:407-8.

4. Bouchart F, Dubar A, Tabley A, et al. Coarctation of the aorta in adults: surgical results and long-term follow-up. Ann Thorac Surg 2000;70:1483-8; discussion 1488-9.

5. Fletcher SE, Nihill MR, Grifka RG, et al. Balloon angioplasty of native coarctation of the aorta: midterm follow-up and prognostic factors. J Am Coll Cardiol 1995;25:730-4.

6. Johnston TA, Grifka RG, Jones TK. Endovascular stents for treatment of coarctation of the aorta: acute results and follow-up experience. Catheter Cardiovasc Interv 2004;62:499-505.

7. Rajasinghe HA, Reddy VM, van Son JA, et al. Coarctation repair using end-to-side anastomosis of descending aorta to proximal aortic arch. Ann Thorac Surg 1996;61:840-4.

8. Younoszai AK, Reddy VM, Hanley FL, et al. Intermediate term follow-up of the end-to-side aortic anastomosis for coarctation of the aorta. Ann Thorac Surg 2002;74:1631-4.

9. LaDisa JF Jr, Dholakia RJ, Figueroa CA, et al. Computational simulations demonstrate altered wall shear stress in aortic coarctation patients treated by resection with end-to-end anastomosis. Congenit Heart Dis 2011;6:432-43.

10. LaDisa JF Jr, Alberto Figueroa C, Vignon-Clementel IE, et al. Computational simulations for aortic coarctation: representative results from a sampling of patients. J Biomech Eng 2011;133:091008.

11. Liu, JL, Itatani K, Shiurba R, et al. Image-based computational hemodynamics of distal aortic arch recoarctation following the Norwood procedure. 4th International Conference on Biomedical Engineering and Informatics (BMEI), 2011:318-23.

12. Liu, JL, Qian Y, Itatani K, et al. An approach of computational hemodynamics for cardiovascular flow simulation. ASME-JSME-KSME 2011 Joint Fluids Engineering Conference, 2011:1449-56.

13. Hong H, Menon PG, Zhang H, et al. Postsurgical comparison of pulsatile hemodynamics in five unique total cavopulmonary connections: identifying ideal connection strategies. Ann Thorac Surg 2013;96:1398-404.

14. Chen Z, Zhou Y, Wang J, et al. Modeling of coarctation of aorta in human fetuses using 3D/4D fetal echocardiography and computational fluid dynamics. Echocardiography 2017;34:1858-66.

15. Goubergrits L, Riesenkampff E, Yevtushenko P, et al. MRI-based computational fluid dynamics for diagnosis and treatment prediction: clinical validation study in patients with coarctation of aorta. J Magn Reson Imaging 2015;41:909-16.

16. Sun Q, Liu J, Qian Y, et al. Computational haemodynamic analysis of patient-specific virtual operations for total cavopulmonary connection with dual superior venae cavae. Eur J Cardiothorac Surg 2014;45:564-9.

17. Mao L, Liu JL, Hong HF, et al. Hemodynamic analysis of surgical correction for patient-specific aortic coarctation with aortic arch hypoplasia by end-to-side anastomosis. 7th International Conference on Biomedical Engineering and Informatics (BMEI), 2014:446-50.